Journal of Solid State Electrochemistry (2022) 26:353–363
https://doi.org/10.1007/s10008-021-05061-2

ORIGINAL PAPER

Electrodeposited molybdenum-doped Co_3O_4 nanosheet arrays for high-performance and stable hybrid supercapacitors

Honglong Shen[1] · Xiaoqiang Yang[1] · Juanjuan Song[1] · Haiwen Gao[1] · Zongdeng Wu[1] · Jia Yu[1] · Wu Lei[1] · Jiazhi Yang[1] · Guangyu He[2] · Qingli Hao[1]

Received: 22 June 2021 / Revised: 27 September 2021 / Accepted: 29 September 2021 / Published online: 10 October 2021

Abstract

Long-cycle stability and high-energy density are big challenges for developing high-performance hybrid supercapacitor (HSC) electrode materials. In this work, molybdenum-doped Co_3O_4 nanosheets arrays on nickel foam (noted as $Mo_xCo_{1.5-x}O$/NF) are successfully prepared via facile one-step electrodeposition followed by annealing for hybrid supercapacitors. The experimental and calculated results indicate that the band gap modification and conductivity enhancement of $Mo_xCo_{1.5-x}O$ lead to excellent capacitive performance due to the doping of Mo into Co_3O_4. The as-prepared $Mo_{0.25}Co_{1.25}$/NF electrode demonstrates a high specific capacity of 128.2 mAh g^{-1} (923 F g^{-1}) at 1 A g^{-1} (60% higher than the undoped Co_3O_4) and superior cycle stability with 95.2% capacity retention after 10,000 cycles at 10 A g^{-1}. The assembled HSC delivers high-energy density of 64.3 Wh kg^{-1} at the power density of 794.1 W kg^{-1} and with 87.7% capacity retention after 10,000 cycles. This work can present a new strategy to fabricate the three-dimensional high-performance integrated electrode materials by a facile electrodeposition for heteroatom-doped transition metal oxide for high-performance supercapacitors.

Keywords Nanosheets · Electrodeposition · Cycle stability · Hybrid supercapacitors · Doping

Introduction

As one of the most potential energy storage devices, supercapacitors are popular in relevant research field because of their fast charge and discharge rates, high power density, long cycle life, and high safety [1]. However, the development and large-scale application for supercapacitors are greatly limited by its low energy density. According to the energy density formula $E = 1/2CV^2$, it can be seen that developing high specific capacity electrode and broadening the work potential window of supercapacitors could greatly improve energy density. Therefore, it is of great significance to develop cathode materials with higher reversible specific capacity for supercapacitors [2].

Transition metal oxides (NiO [3], MnO_2 [4], Co_3O_4 [5]) are most widely studied and reported cathode materials for supercapacitors for the advantages of high specific capacity, good structural stability, low cost, non-toxicity, and abundant natural resources [6]. Among these transition metal oxides, Co_3O_4 is considered as an ideal cathode material for supercapacitors due to its high theoretical specific capacity (333.9 mAh g^{-1}), unique nanostructure, and environmental friendliness [7]. However, single metal oxide Co_3O_4 as cathode material for supercapacitors usually exhibits poor electronic conductivity and cycle life as well as the lower specific capacity (far below the theoretical specific capacity), which limits its large-scale application [8]. Guan et al. [9] prepared needle-like Co_3O_4 for supercapacitors with the capacity of 26.2 mAh g^{-1} at 0.1 A g^{-1} and 70% capacity retention after

Highlights
(1) Mo doped Co_3O_4 nickel foam electrodes ($Mo_xCo_{1.5-x}O$/NF) are synthesized by electrodeposition.
(2) The effect of Mo doping on the bandgap of Co_3O_4 and electrochemical properties was studied.
(3) $Mo_{0.25}Co_{1.25}O$/NF exhibits high specific capacity and superior capacity retention of 95.2% after 10000 cycles.
(4) The HSC device shows energy density of 64.3 Wh kg^{-1} at 794.1 W kg^{-1}.

✉ Qingli Hao
qinglihao@njust.edu.cn

[1] Key Laboratory for Soft Chemistry and Functional Materials, Ministry of Education, School of Chemical Engineering, Nanjing University of Science and Technology, NanjingJiangsu 210094, China

[2] Jiangsu Key Laboratory of Advanced Catalytic Materials and Technology, Changzhou University, Changzhou 213164, China

1000 cycles at 0.2 A g^{-1}. In order to compensate for the shortcoming mentioned above, the conductivity of Co_3O_4 can be improved by combining with carbon materials [10], conductive polymers [11], and conductive metal oxide/sulfide [12, 13]. However, the introduction of carbon would greatly decrease the specific capacity of Co_3O_4. Some reports showed that metal elements doping can adjust the band gap and enhance the conductivity and capacity of electrode materials effectively. Zhang et al. [14] synthesized Fe-doped Co_3O_4 through hydrothermal followed by a post-heat treatment for supercapacitors with the capacity of 277.3 mAh g^{-1} and 86.9% capacity retention after 5000 cycles at 20 A g^{-1}. Recently, our group developed Mn-doped Co_3O_4 mesoporous nanoneedle array via hydrothermal method combined with annealing for supercapacitors, with the specific capacity of 102.1 mAh g^{-1} at 1 A g^{-1} and long cycle stability of 104% capacity retention after 10,000 cycles [15]. However, there are little research on the preparation of heteroatom-doped Co_3O_4 by a more convenient and environmental method. Electrodeposition is often used to build integrate electrodes due to the strong adhesion between the active materials and current collectors [16, 17]. For instance, Huang et al. [18] prepared Al-doped CoS by electrodeposition method for supercapacitors with improved electrochemical activity.

Herein, we have firstly synthesized a novel electrode based on Mo-doped Co_3O_4 3D nanosheets arrays on nickel foam (NF) through one-step electrodeposition method followed by annealing in air. The calculated bandgap results of Mo-doped Co_3O_4 showed that its band gap could be modified and its conductivity could be enhanced by Mo doping, resulting in excellent capacity performance. The $Mo_{0.25}Co_{1.25}$/NF demonstrated a high specific capacity of 128.2 mAh g^{-1} (923 F g^{-1}) at 1 A g^{-1} (higher than that of undoped Co_3O_4, 80.4 mAh g^{-1}) and superior cycle stability with 95.2% capacity retention after 10,000 cycles at 10 A g^{-1}. The assembled hybrid supercapacitor (HSC), $Mo_{0.25}Co_{1.25}O$/NF//KOH//N-doped carbon/carbon cloth (N-C/CC), exhibited a high specific capacity 81.5 mAh g^{-1} (586.8 F g^{-1}) at 1 A g^{-1} and achieved a high-energy density of 64.3 Wh kg^{-1} at 794.1 W kg^{-1}, as well as excellent cycle stability with 87.7% capacity retention after 10,000 cycles. The great enhancement in electrochemical performance is contributed to the effective doping of Mo element, the porous structure of $Mo_xCo_{1.5-x}O$, and the 3D heterogenerous architecture.

Experiment

Treatment of nickel foam

Nickel foam (NF) purchased from Jiangsu Kunshan Guangjiayuan Company. The original specification of nickel foam is 250 mm × 1000 mm × 1.5 mm. Nickel foam was soaked in 3M HCl for 10 min; then rinsed with deionized water for 3 times; then soaked in acetone, ethanol, and deionized water for 15 min; and then rinsed 3 times with anhydrous alcohol and dried at room temperature.

Fabrication of $Mo_xCo_{1.5-x}O$/NF

In the experiment, the total molar amount (1.5 mM) of the $Co(NO_3)_2{\cdot}6H_2O$ and $Na_2MoO_4{\cdot}2H_2O$ was unchanged. Various integrated electrodes were electrodeposited on NF under the same condition by changing the amount (0.75, 0.5, 0.25, 0.125, and 0 mM) of Na_2MoO_4. The electrodes were noted as $Mo_xCo_{1.5-x}O$/NF ($x = 0$, 0.125, 0.25, 0.5, and 0.75).

Corresponding molar mounts of $Co(NO_3)_2{\cdot}6H_2O$ and $NaMo_2O_4{\cdot}2H_2O$ were dissolved in 25 mL deionized water by constant vigorous stirring (1 h). KCl (2.5 mM) was added into the above solution and stirred for extra one hour as electrolyte. The metal hydroxide precursor was electrodeposited on NF in a standard three-electrode system. The NF (1 × 1.5 cm^2), platinum sheet, and the Ag/AgCl were used as the work electrode, the counter electrode, and the reference electrode, respectively. Cyclic voltammetry (CV) was performed at the scan rate of 50 mV s^{-1} for 60 cycles within a voltage window of −1.2~0.2 V (vs Ag/AgCl). The obtained electrodes were repeatedly rinsed with deionized water and dried at 60 °C for 6 h. Finally, the as-prepared hydroxide samples were annealed at 350 °C for 2 h in air. The loading mass of $Mo_xCo_{1.5-x}O$/NF ($x = 0$, 0.125, 0.25, 0.50, and 0.75) electrodes was 1.8, 1.2, 0.9, 0.7, and 0.5 mg cm^{-2}, respectively.

Characterization

The X-ray diffraction (XRD, Bruker D8-Advance diffractometer) of $Mo_xCo_{1.5-x}O$/NF was performed with Cu Kα radiation. The corresponding element valence and distribution of electrodes were investigated by X-ray photoelectron spectrometer (XPS, Thermo-VG Scientific ESCALAB 250X). The morphology of the materials was identified by field emission scanning electron microscopy (FE-SEM, JSM-IT500HR) with energy-dispersive X-ray (EDX) and transmission electron microscopy (TEM, JEOL JEM2100 PLUS).

Electrochemical measurements

The electrochemical tests including cyclic voltammetry (CV), galvanostatic charge-discharge (GCD), and electrochemical impedance spectroscopy (EIS) were performed on an electrochemical workstation (Wuhancorr Test) at room temperature in three-electrode or two-electrode system. The long-term cycling stability was measured with the LAND battery test system (Wuhan Rambo Testing

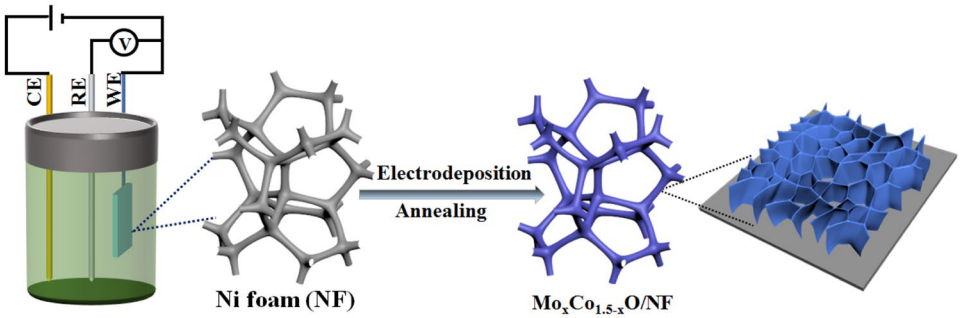

Fig. 1 Schematic diagram of $Mo_xCo_{1.5-x}$/NF synthesis

Equipment Co. Ltd). The as-prepared $Mo_xCo_{1.5-x}O$/NF was used as the working electrode, platinum sheet was used as the counter electrode, Hg/HgO was used as the reference electrode, and 6 M KOH solution was used as electrolyte, respectively. The hybrid supercapacitor (HSC) was assembled with $Mo_{0.25}Co_{1.25}O$/NF as cathode and N-C/CC as anode. The cellulose was chosen as separator, and 2 M KOH solution was used as electrolyte in the HSC. The specific capacity of electrodes was calculated according to Eq. (1) [6]:

$$Q = \frac{I\Delta t}{3.6m} \tag{1}$$

Here, Q (mAh g^{-1}) is the specific capacity, I (A) is the discharge current, and Δt (s) and m (g) represent the discharge time and the loading mass of the active material, respectively.

The mass of the cathode and anode was determined according to the following Eq. (2) [6]:

$$\frac{m_+}{m_-} = \frac{Q_-}{Q_+}\frac{\Delta V}{\Delta V_+} \tag{2}$$

In which, $m_+(m_-)$, $Q_+(Q_-)$, and $\Delta V_+(\Delta V_-)$ are the loading mass, the specific capacity, and the absolute value of the discharge potential windows of cathode (anode), respectively. The total loading mass of cathode and anode is about 2.2 mg.

The energy density (E) and power density (P) of the HSC were calculated by the following Eqs. (3) and (4) [7]:

$$E = \frac{1}{2}QV \tag{3}$$

$$P = 3600\frac{E}{\Delta t} \tag{4}$$

where Q (mAh g^{-1}), V (V), and Δt (s) represent the specific capacity, potential window, and the discharge time of the HSC, respectively.

Results and discussion

Structure characterization

The synthesis process of $Mo_xCo_{1.5-x}O$/NF is depicted in the Fig. 1, which contains a facile electrodeposition and an annealing treatment. Na_2MoO_4 was selected as the Mo source. As an inorganic salt, KCl can improve the conductivity of the electrolyte.

The phase and structure of $Mo_xCo_{1.5-x}O$/NF (x = 0, 0.125, 0.25, 0.5, and 0.75) were determined by the XRD. In the Fig. 2a, there are several obvious diffraction peaks at 19.0°, 31.0°, 36.9°, 38.6°, 44.9°, 55.7°, 59.5°, and 65.4°, which can be indexed to the (111), (220), (311), (222), (400), (422), (511), and (440) crystal planes of Co_3O_4, respectively (JCPDS card no.74-1656). The peaks at 44.21°, 51.25°, and 75.92° are the strong diffraction peaks of Ni foam. The major peak (311) of all $Mo_xCo_{1.5-x}O$/NF ($x > 0$) electrodes

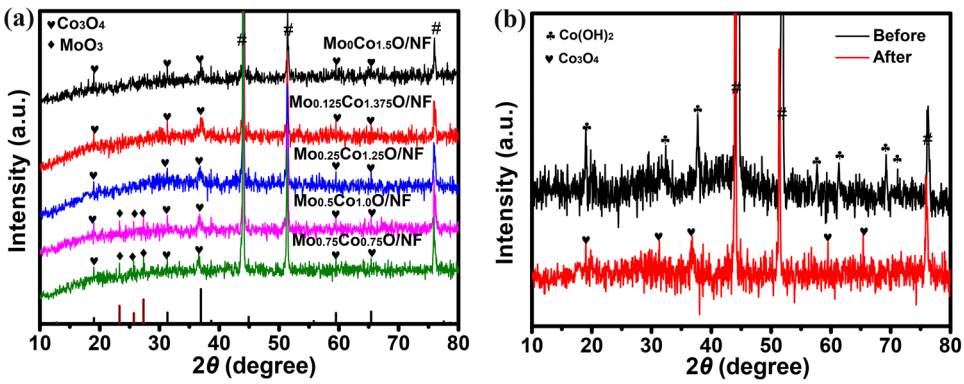

Fig. 2 **a** XRD of $Mo_xCo_{1.5-x}O$/NF; **b** XRD of $Mo_{0.25}Co_{1.25}O$/NF before and after annealing

shows a slight shift due to Mo doping. However, the diffraction peaks at 23.32°, 25.70°, and 27.33° attributed to orthorhomhic structure of MoO_3 (JCPDS crad no.05-0508) are observed when the Na_2MoO_4 amount is more than 0.5 mM for $Mo_xCo_{1.5-x}O$/NF (x = 0.5 and 0.75). The XRD result of $Mo_{0.25}Co_{1.25}O$/NF before annealing is presented in Fig. 2b. The peaks at 19.0°, 32.4°, 37.7°, 57.7°, 61.3°, 69.2°, and 71.1° corresponding to (001), (100), (101), (110), (111), (103), and (201) planes of $Co(OH)_2$ (JCPDS card no.03-0913), respectively. Moreover, no diffraction peaks of molybdenum oxide could be detected in $Mo_{0.25}Co_{1.25}O$ samples due to the amorphous molybdenum oxide [19].

The morphologies of all electrodes were observed by SEM. As shown in Fig. 3a–c, the abundant nanosheets of $Mo_{0.25}Co_{1.25}O$ with a thickness about 50nm assemble nanosheet arrays on the top of 3D NF substrate. This structure provides vast active sites for electrochemical reactions. While for the other $Mo_xCo_{1.5-x}O$/NF electrodes, all the electrodes are composed of nanoparticles growing on 3D NF skeletons (Fig. S1). When the content of Mo source increases from 0 to 0.25 mM, the morphology of the materials presents the nanosheet array structure consisted of numerous nanoparticles. While the content of Mo source increases to 0.5 and 0.75 mM, the nanoparticles begin to agglomerate and the nanosheet arrays are not obvious. Therefore, according to the SEM results of all $Mo_xCo_{1.5-x}O$/NF electrodes, we can determine that the $Mo_{0.25}Co_{1.25}O$/NF electrode has a better morphology than the other electrodes. Figure 3d shows the SEM mapping of Co, O, and Mo elements in the $Mo_{0.25}Co_{1.25}O$/NF electrode. Obviously, the Co, O, and Mo elements are homogenous distributed on the whole integrated electrode, and the SEM mapping results show that the atom content for Co, O, and Mo elements is 34.0%, 59.8%, and 6.2%, respectively, which indicates that molybdenum is successfully introduced to the electrode.

The morphology of $Mo_{0.25}Co_{1.25}O$/NF was further characterized by TEM. Figure 4a, b show the ultra thin $Mo_{0.25}Co_{1.25}O$ nanosheets with wrinkles. Moreover, there are many nanopores in the nanosheets, which result from the release of H_2O molecules during the heat treatment process at high temperature [20, 21]. From the high-resolution TEM (HRTEM) shown in Fig. 4c, the lattice fringes of $Mo_{0.25}Co_{1.25}O$/NF nanosheets are measured to be 0.249, 0.206, and 0.142 nm, which well match with the (311), (400), and (440) planes of Co_3O_4 (JCPDS:74-1656), respectively. The selected area electron diffraction (SAED) pattern of $Mo_{0.25}Co_{1.25}O$/NF (Fig. 4d) shows ring patterns which indicate their polycrystalline structure and each diffraction ring can also be well indexed into crystal faces of Co_3O_4.

The elemental composition and valence state of $Mo_{0.25}Co_{1.25}O$/NF were investigated by XPS. The survey spectrum (Fig. 5a) shows that $Mo_{0.25}Co_{1.25}O$/NF consists of Mo, O, Co, Ni, and C elements, in which the element Ni and C derive from NF and the conductive tape used to fix samples, respectively. The Co 2p XPS spectrum (Fig. 5b) has two main peaks and their satellites peaks. The fitting peaks at 779.75 and 794.85 eV are corresponded to Co^{3+}, while the peaks at 780.3 and 796.1 eV are related to Co^{2+}, respectively. The result indicates that cobalt of $Mo_{0.25}Co_{1.25}O$

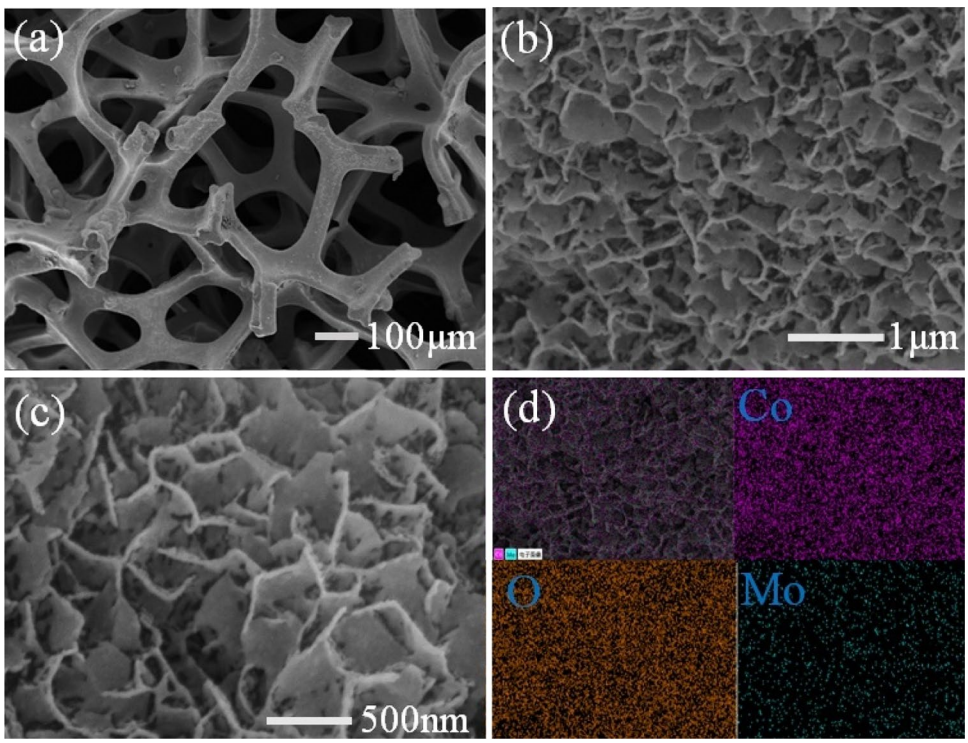

Fig. 3 **a–c** SEM images and **d** corresponding element mapping of $Mo_{0.25}Co_{1.25}O$/NF

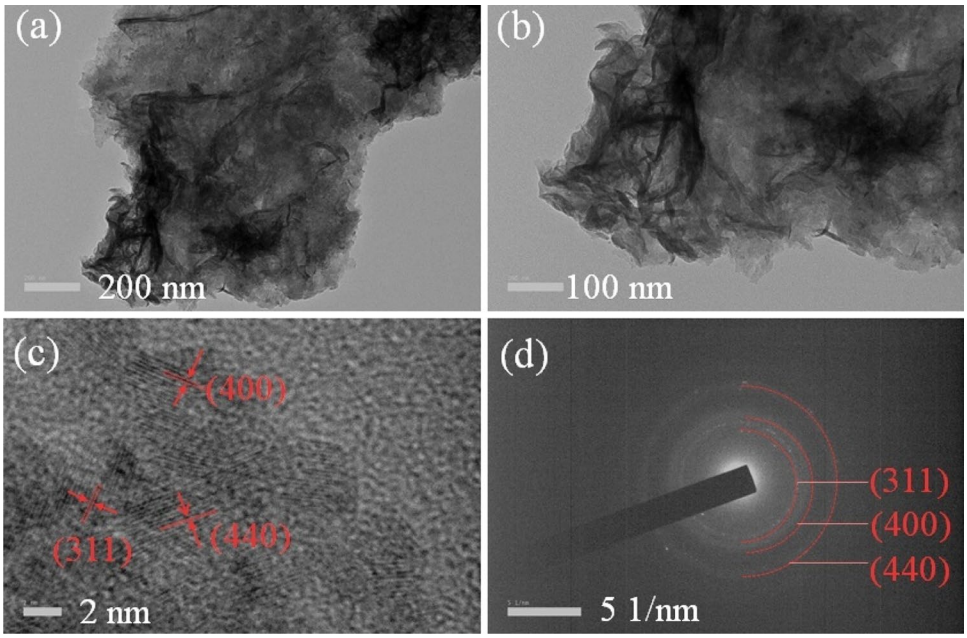

Fig. 4 **a**, **b** TEM images, **c** HRTEM, and **d** SAED pattern of $Mo_{0.25}Co_{1.25}O$/NF

exists in the form of Co_3O_4. However, these binding energy values of $Co^{3+}$and Co^{2+} are a little different from those of pure Co_3O_4 reported in the literature [15, 22], which is probably due to the charge redistribution of the materials in the presence of Mo atoms.

As shown in Fig. 5c, the significant spectrum of Mo 3d has two main peaks located at 235.1 eV (Mo $3d^{3/2}$) and 231.8 eV (Mo $3d^{1/2}$). The fitting peaks at 235.1 and 231.8 eV correspond to Mo^{6+}, which prove the successful introduction of Mo source [23, 24]. The fitting peaks of O 1s spectrum (Fig. 5d) at 529.5 eV (O1), 531.2 eV (O2), and 533.2 eV (O3) are related to M–O, OH^-, and absorbed water in the $Mo_{0.25}Co_{1.25}O$/NF electrode, respectively [25].

Electrochemical performance

The CV curves of all $Mo_xCo_{1.5-x}O$/NF electrodes at 5 mV s^{-1} with the potential window of 0~0.6 V (vs Hg/HgO) are shown in Fig. 6a. For the $Mo_0Co_{1.5}O$/NF electrode, a pair of low intensity redox peaks at 0.446 V and 0.247 V can be attributed to the Co^{2+}/Co^{3+} and Co^{3+}/Co^{4+} redox process, respectively [26]. With the addition amount of Mo increases from 0 to 0.25 mM, the potential positions of these redox peaks gradually shift negatively and positively, meaning that the redox reaction is getting easier due to the introduction of Mo. However, when the amount of Na_2MoO_4 increases from 0.25 to 0.75 mM, the redox peak potential begins to increase compared with $Mo_{0.25}Co_{1.25}O$/NF electrode. It indicates that the reaction of the $Mo_xCo_{1.5-x}O$/NF electrode becomes difficult when the Na_2MoO_4 is added more, and the $Mo_{0.25}Co_{1.25}O$/NF electrode needs the minimum energy compared to the other electrodes.

To exclude the effect of NF on capacity, the bared NF was also tested under the same conditions (Fig. S2a). Compared to all $Mo_xCo_{1.5-x}O$/NF electrodes, the bare NF almost exhibits no integrated area, indicating the low capacity contribution from the NF (Fig. S2a).

The integrated area of all $Mo_xCo_{1.5-x}O$/NF (x = 0, 0.125, 0.25, 0.5, 0.75) electrodes are calculated to be 1.488, 3.798, 4.388, 4.301, and 3.571, respectively, manifesting that the $Mo_{0.25}Co_{1.25}O$/NF electrode has the highest specific capacity. The HOMO and LUMO values of all $Mo_xCo_{1.5-x}O$/NF electrodes were investigated based on Eqs. (5) and (6), in which E_{onset}^{ox} and E_{onset}^{red} stand for the onset oxidation peak potential and the reduction peak potential. $E_{ox\ (ferrocene)}$ is the oxidation peak (0.38 V vs Ag/AgCl) of ferrocene [27]. All potentials (vs Hg/HgO) were converted to values vs Ag/AgCl by adding 0.054 V. The HOMO values of all $Mo_xCo_{1.5-x}O$/NF (x = 0, 0.125, 0.25, 0.5, and 0.75) were estimated to be −4.841, −4.860, −4.753, −4.853, and −4.839 eV, respectively. The LUMO values of all $Mo_xCo_{1.5-x}O$/NF (x = 0, 0.125, 0.25, 0.5, and 0.75) were also evaluated to be −4.798, −4.829, −4.748, −4.836, and −4.820 eV, respectively. In addition, the calculated bandgaps (E_g^{CV}) of all $Mo_xCo_{1.5-x}O$/NF (x = 0, 0.125, 0.25, 0.5, and 0.75) electrodes based on Eq. (7) are −0.043, −0.031, −0.005, −0.017, and −0.019 eV, respectively. The above results indicate that the additional electronic effect of the composites is caused when the Mo^{6+} is introduced into Co_3O_4 ($Mo_0Co_{1.5}O$), which leads to the decrease of the bandgaps of all $Mo_xCo_{1.5-x}O$/NF (x > 0)

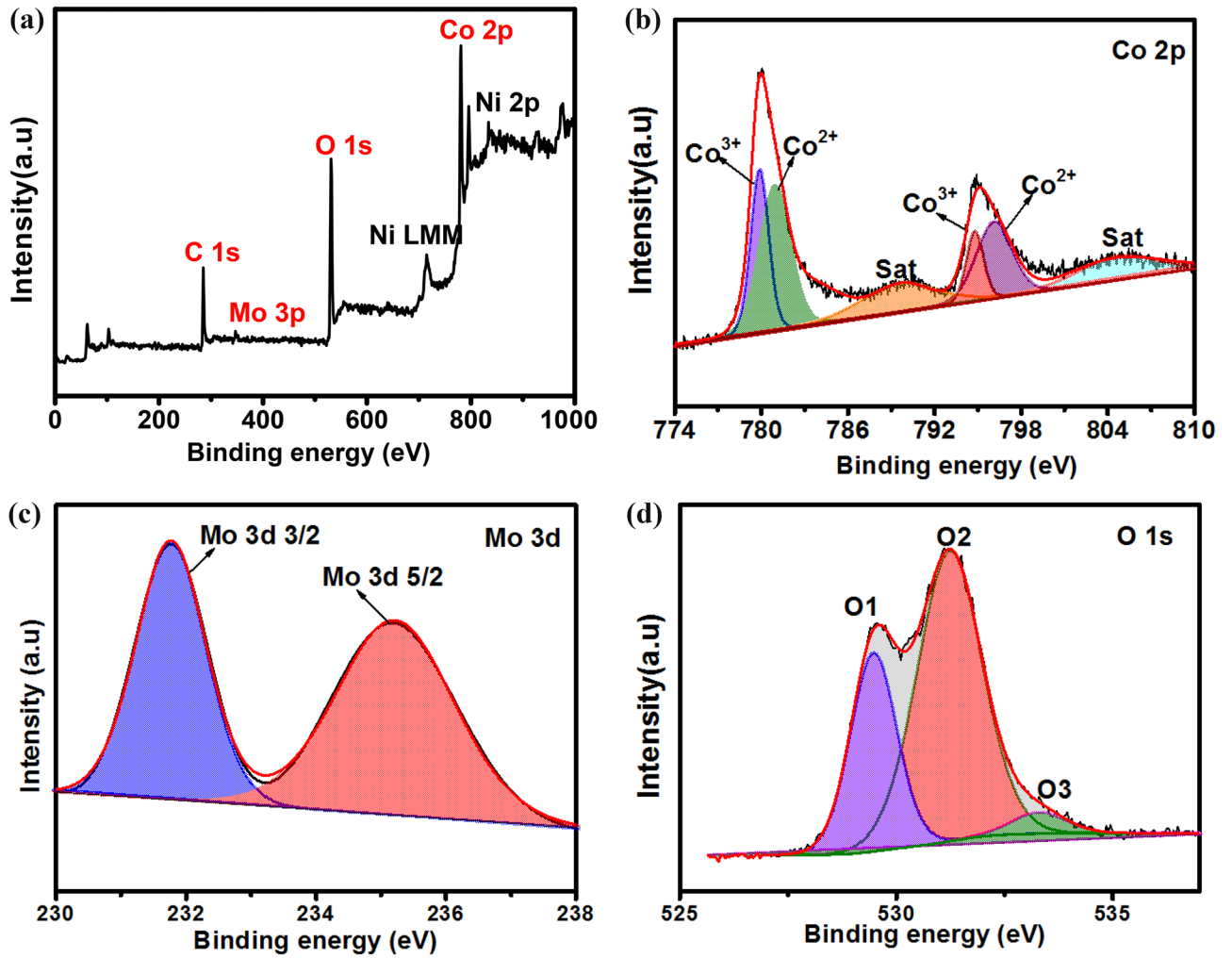

Fig. 5 XPS spectrum of $Mo_{0.25}Co_{1.25}O$/NF (**a**), XPS survey spectra of Co 2p (**b**), Mo 3d (**c**), and O 1s (**d**)

electrodes. Notably, $Mo_{0.25}Co_{1.25}O$/NF exhibits the lowest bandgap due to the optimal Mo^{6+} ions doping.

$$\mathrm{HOMO} = -\left[E^{\mathrm{ox}}_{\mathrm{onset}} - E_{\mathrm{ox(ferrocene)}}\right] - 4.8 \quad (5)$$

[27]

$$\mathrm{LUMO} = -\left[E^{\mathrm{red}}_{\mathrm{onset}} - E_{\mathrm{ox(ferrocene)}}\right] - 4.8 \quad (6)$$

[27]

$$E_g^{CV} = HOMO - LUMO \quad (7)$$

[27]

As shown in Fig. 6b, the $Mo_{0.25}Co_{1.25}O$/NF electrode exhibits the better rate performance (83.2%) than other $Mo_xCo_{1.5-x}O$/NF electrodes (83.0%, 81.9%, 80.6%, and 55.3%) for $x = 0.75$, 0.5, 0.125, and 0, respectively.

The $Mo_{0.25}Co_{1.25}O$/NF electrode exhibits a pair of peaks at 0.355 V and 0.224 V related to the faradaic reaction of Co_3O_4 in KOH electrolyte at 5 mV s^{-1} (Fig.6c). Moreover, even at a high scan rate of 50 mV s^{-1}, the CV curves of $Mo_{0.25}Co_{1.25}O$/NF electrode still have obvious redox peaks and keep the similar shape to that at 5 mV s^{-1}. The Mo source only improved the stability of the $Mo_xCo_{1.5-x}O$/NF ($x > 0$) electrodes, but did not participate in the redox reaction related to OH^-. The corresponding redox reactions are presented in the Eqs. (8) and (9) [12, 30].

$$Co_3O_4 + OH^- + H_2O \leftrightarrow 3CoOOH + e^- \quad (8)$$

$$CoOOH + OH^- \leftrightarrow CoO_2 + H_2O + e^- \quad (9)$$

The charge time and discharge time of $Mo_{0.25}Co_{1.25}O$/NF electrode at the same current density are almost equal (Fig. 6d), which indicates that the $Mo_{0.25}Co_{1.25}O$/NF has better faradaic reaction reversibility and rapid I-V response. The calculated specific capacity of $Mo_{0.25}Co_{1.25}O$/NF electrode is 128.2 mAh g^{-1} (923 F g^{-1}) at 1 A g^{-1}. The cycling performance of all $Mo_xCo_{1.5-x}O$/NF electrodes at 10 A g^{-1} for 1000 cycles is also investigated (Fig. S2b). The capacity retention of $Mo_xCo_{1.5-x}O$/NF ($x = 0$, 0.125, 0.25, 0.5, 0.75) is 61.7%, 89.4%, 100.6%, 84.2%, and 80.2% at 10 A g^{-1}

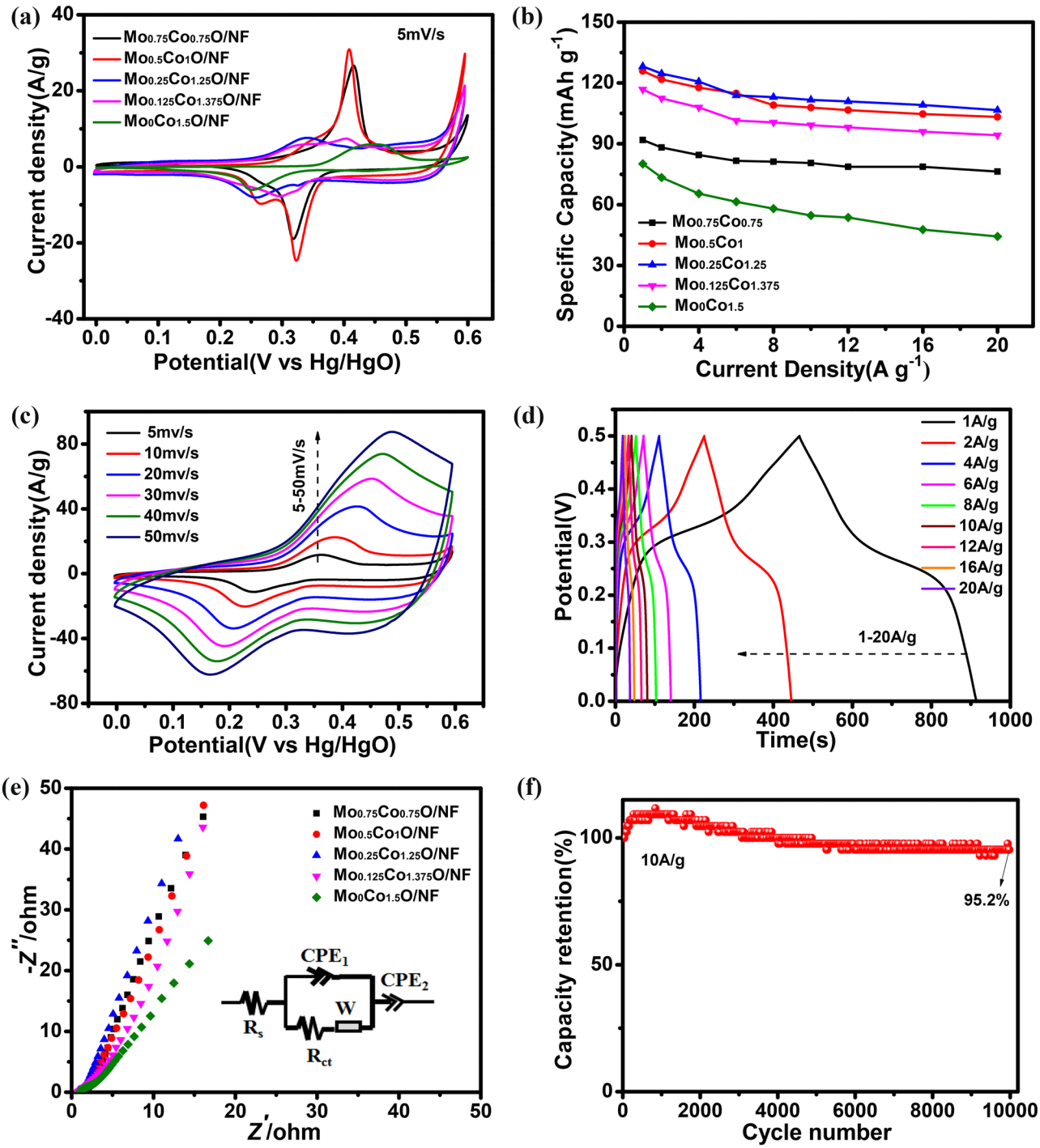

Fig. 6 CV curves (**a**) and rate performance (**b**) of $Mo_xCo_{1.5-x}O$/NF electrodes, CV curves (**c**) and GCD curves (**d**) of $Mo_{0.25}Co_{1.25}O$/NF electrode, EIS curves of $Mo_xCo_{1.5-x}O$/NF electrodes and the equivalent circuit (**e**), and cycling performance of $Mo_{0.25}Co_{1.25}O$/NF electrode (**f**)

after 1000 cycles, respectively. Obviously, the cycle stability of $Mo_xCo_{1.5-x}O$/NF electrodes is significantly improved when the Mo is added into Co_3O_4/NF [19, 31].

Figure 6e demonstrates that each $Mo_xCo_{1.5-x}O$/NF electrode presents a small charge transfer resistance (*Rct*) corresponding to semicircular arc in the high-frequency region and diffusion resistance relate to the slope of line in the low-frequency region [28, 29]. The EIS curves of all $Mo_xCo_{1.5-x}O$/NF electrodes were fitted by using ZView software. The results reveal that the *Rct* values of $Mo_0Co_{1.5}O$/NF, $Mo_{0.125}Co_{1.375}O$/NF, $Mo_{0.25}Co_{1.25}O$/NF, $Mo_{0.5}Co_1O$/NF, and $Mo_{0.75}Co_{0.75}O$/NF electrodes are 4.196, 1.996, 0.618, 1.615, and 2.518 Ω, respectively (Table S1). Obviously, the $Mo_{0.25}Co_{1.25}O$/NF electrode

exhibits the minimum *R*ct and diffusion resistance among all $Mo_xCo_{1.5-x}O$/NF electrodes. This result further verifies that the appropriate doping of Mo source in Co_3O_4 greatly changes its electronic state and accelerates the electron transfer rate. Therefore, $Mo_{0.25}Co_{1.25}O$/NF exhibits the smallest bandgap and the best electrochemical performance.

The cycling stability of as-prepared $Mo_{0.25}Co_{1.25}O$/NF electrode was measured by GCD for 10,000 cycles at 10 A g^{-1} (Fig. 6f). Initially, the capacity of $Mo_{0.25}Co_{1.25}O$/NF gradually increases due to the activation of electrode. The capacity retention starts to decrease when it reaches 3500 cycles, which is caused by the microstructure change of the electrode. The capacity retention of the $Mo_{0.25}Co_{1.25}O$/NF electrode is 95.2% after 10,000 cycles. The $Mo_{0.25}Co_{1.25}O$/NF electrode has a larger *R*ct and diffusion resistance after 10,000 cycles (Fig. S3), which is probably caused by the slight change in microstructure of the active materials during 10,000 cycles. Therefore, as perior electrochemical material, the $Mo_{0.25}Co_{1.25}O$/NF in this work is more competitive than the most reported electrode materials listed in Table 1.

Figure S4 shows the SEM images of $Mo_{0.25}Co_{1.25}O$/NF electrode after 10,000 cycles. The microstructure of the $Mo_{0.25}Co_{1.25}O$/NF electrode remains stable without obvious change even after 10,000 cycles. The SEM mapping results show that the atom content for Co, O, and Mo elements is 33.2%, 60.7%, and 6.1%, respectively, which is consistent with the original result.

It is believed that the following aspects may be accounted for the high electrochemical performance and excellent cycling stability of $Mo_{0.25}Co_{1.25}O$/NF electrode for supercapacitors. Firstly, the binder-free feature and Mo source doping can enhance the conductivity of as-prepared electrode, which facilitates the fast charge transportation. Secondly, the nanosheetarrays provide numerous active sites for redox reactions. Thirdly, the interconnect nanosheet arrays on NF provide a stable structure and shorten the diffusion path of ions and electrons. Finally, Co element is responsible for providing high capacity and Mo element is responsible for improving the stability of the electrode [31, 32].

Hybrid supercapacitor device

The hybrid supercapacitor (HSC) was assembled by employing $Mo_{0.25}Co_{1.25}O$/NF as the cathode and N-C/CC as the anode (noted as $Mo_{0.25}Co_{1.25}O$/NF/KOH//N-C/CC), and the schematic diagram is shown in Fig. 7a. The electrochemical performance of N-C/CC is showen in Fig. S5. Their CV curves of HSC at 5 mV s^{-1} in a three-electrode system are presented in Fig. S6a. Different potential was also applied to determine the optimized operating voltage of the HSC, as shown in Fig. S6b. The shape of CV curves (Fig. 7b) shows quasi-rectangular, which indicates that the capacity contribution of HSC mainly comes from the capacitive behaviour. With the current density increasing from 1 to 20 A g^{-1}, there are no obvious voltage platform in GCD curves (Fig. 7c). As shown in Fig. 7d, the calculated specific capacity of HSC based on Eq. (1) is 81.5, 73.1, 62.7, 53.3, 46.1, and 42.5 mAh g^{-1} at the current density of 1, 2, 5, 10, 15, and 20 A g^{-1}, respectively.

The cycling performance of the HSC is shown in Fig. 7e. The capacity retention of the HSC is 87.7% after 10,000 cycles. Meanwhile, two HSCs connected in series can light up a white LED for 3.5 min. The result proves that the assembled HSC has a superior electrochemical performance than the most reported supercapacitors assembled with Co/Mo-based composite materials [7, 8, 19, 33].

Figure 7 f is the relationship between energy and power density of the HSC. The HSC achieved high-energy density of 64.3 Wh kg^{-1} at 794.1 W kg^{-1} and high power density of 13.79 kW kg^{-1} at 25.2 Wh kg^{-1}, which is comparable to

Table 1 Brief capacity and cycling performance list of cobalt- and molybdenum-based materials for SCs in literature

Material	Capacity	Current density	Cycling performance	Reference
Mo-Co-S	85.7 mAh g^{-1}	2 A g^{-1}	109%,30000 cycles	[6]
Co_3O_4@$NiMoO_4$	226.7 mAh g^{-1}	0.5 A g^{-1}	72%, 3000 cycles	[11]
Co_3O_4@$CoMoO_4$	95.2 mAh g^{-1}	0.5 A g^{-1}	100%, 3000 cycles	[11]
Co_3O_4	58.3 mAh g^{-1}	1 A g^{-1}	93.7%, 10,000 cycles	[12]
Co_3O_4-RGO	88.3 mAh g^{-1}	1A g^{-1}	97.6%, 1000 cycles	[14]
Co_3O_4@ppy	1.8 mAh cm^{-2}	50 mA cm^{-2}	98%, 5000 cycles	[15]
Co_3O_4@$NiCo_2S_4$	10.9 mAh cm^{-2}	8 mA cm^{-1}	97.3%, 5000 cycles	[16]
Mn dope Co_3O_4	102.1 mAh g^{-1}	1 A g^{-1}	104%, 10,000cycles	[17]
$CoMoO_4$@Co_3O_4	146.0 mAh g^{-1}	0.6 A g^{-1}	81.4%,5000 cycles	[28]
$CoMoO_4$@NiCo-LDH	281.1 mAh g^{-1}	1 A g^{-1}	90.8%,5000 cycles	[33]
$CoMoO_4$/MnO_2	250 mAh g^{-1}	1 A g^{-1}	98.6%,10,000 cycles	[34]
Mo doped Co_3O_4	128.2 mAh g^{-1}	1 A g^{-1}	95.2%, 10,000 cycles	This work

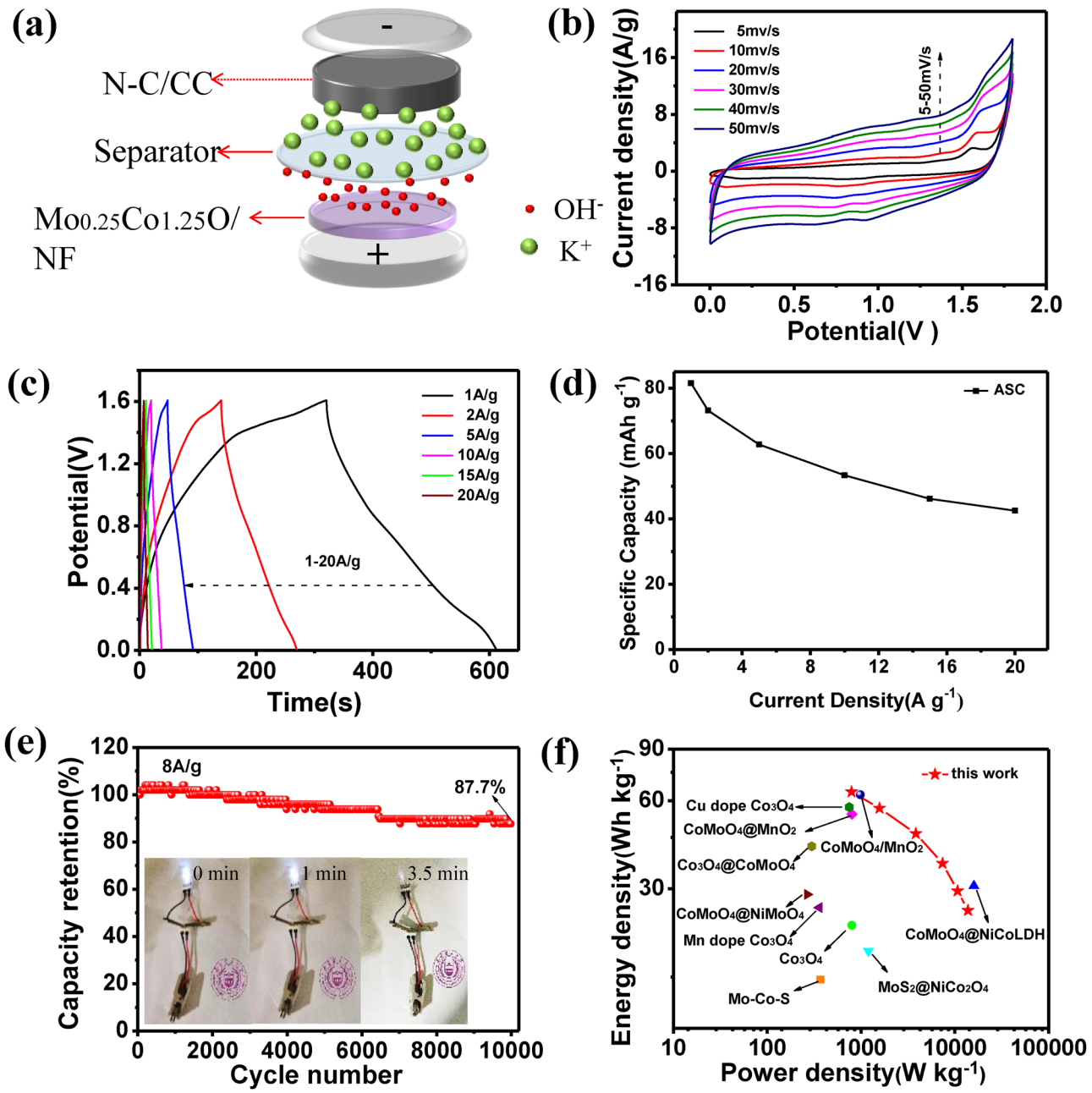

Fig. 7 **a** Schematic of the HSC ($Mo_{0.25}Co_{1.25}O$/NF//N-C/CC), **b** CV curves, **c** GCD curves, **d** rate performance, **e** cycling performance and insert is the light display, and **f** Ragone plots of the HSC

the most reported cobalt and molybdenum based materials previously, such as Cu-doped Co_3O_4@CC//Fe_2O_3@CC (57.1 Wh kg^{-1} at 749.75 W kg^{-1}) [7], Mo-Co-S/CC//AC (14.68 Wh kg^{-1} at 369 W kg^{-1}) [19], $CoMoO_4$@$NiMoO_4$// AC (28.7 Wh kg^{-1} at 267 W kg^{-1}) [24], CC@$CoMoO_4$@ NiCo-LDH//AC (30.7 Wh kg^{-1} at 16000W kg^{-1}) [33], and CoMoO4/MnO_2/NF//M-CNTF (62.9 Wh kg^{-1} at 984 W kg^{-1}) [34].

Conclusions

In summary, we have successfully introduced Mo atoms into Co_3O_4 to construct the integrated electrode ($Mo_xCo_{1.5-x}O$/ NF) composed of porous nanosheet arrays through a facile one-step electrodeposition methods followed by an annealing treatment. The optimized $Mo_{0.25}Co_{1.25}O$/NF electrode demonstrates a high specific capacity of 128.2 mAh g^{-1} (923

F g^{-1}) at 1 A g^{-1} and 95.2% capacity retention after 10,000 cycles. The assembled $Mo_{0.25}Co_{1.25}O$/NF//KOH//N-C/CC HSC device delivers a high-energy density (64.3 Wh kg^{-1} at 794.1 W kg^{-1}) and the capacity retention of 87.7% after 10,000 cycles. In addition, two series of HSCs light up a white LED for 3.5 min. The improvement of electrochemical performance is mainly attributed to the following aspects. Firstly, the band gap and conductivity of Co_3O_4 can be adjusted by Mo doping; secondly, the 3D hierarchical structucture has many interconnected nanosheets of $Mo_xCo_{1.5-x}O$ and porous nanosheets can provide large specific surface area, more active sites, and shorten ion diffusion paths. This work proposes a facile, low cost, and environment friendly strategy of electrodeposion for preparing high-performance electrodes in energy storage systems.

Original statement

1. Mo-doped Co_3O_4 integrated electrodes were prepared by electrodeposition and annealing.
2. The effect of Mo doping on the bandgap of Co_3O_4 and electrochemical properties was studied.

Supplementary information The online version contains supplementary material available at https://doi.org/10.1007/s10008-021-05061-2.

Acknowledgements We also thank the support of the Analysis and Test Center, Nanjing University of Science and Technology, for XRD data collection.

Funding The work was supported by the National Natural Science Foundation of China (Nos. 51972173, 51872140), "333 program" of Jiangsu Province (BRA2019262), Jiangsu Key Laboratory of Advanced Catalytic Materials and Technology (BM2012110), and the program for Science and Technology Innovative Research Team in Universities of Jiangsu Province, China.

Declarations

Conflict of interest The authors declare no competing financial interest.

References

1. Wang Y, Xia Y (2013) Recent progress in supercapacitors: from materials design to system construction. Adv Mater 25:5336–5342
2. Zuo W, Li R, Zhou C et al (2017) Battery-Supercapacitor hybrid devices: recent progress and future prospects. Adv Sci (Weinh) 4:1600539
3. He M, Cao L, Li W et al (2021) NiO nanoflakes decorated needle-like $MnCo_2O_4$ hierarchical structure on nickle foam as an additive-free and high performance supercapacitor electrode. J Mater Sci 56:8613–8626
4. Zhao X, Liu X, Li F et al (2020) MnO_2@NiO nanosheets@nanowires hierarchical structures with enhanced supercapacitive properties. J Mater Sci 55:2482–2491
5. Cao Y, Zhang D, Kong X et al (2021) Multi-vacancy Co_3O_4 on nickel foam synthesized via a one-step hydrothermal method for high-efficiency electrocatalytic benzyl alcohol oxidation. J Mater Sci 56:6689–6703
6. Ouyang Y, Huang R, Xia X et al (2019) Hierarchical structure electrodes of NiO ultrathin nanosheets anchored to $NiCo_2O_4$ on carbon cloth with excellent cycle stability for asymmetric supercapacitors. Chem Eng J 355:416–427
7. Chen Y, Hu H, Wang N et al (2019) Cu(I)/Cu(II) partially substituting the Co(II) of spinel Co_3O_4 nanowires with 3D interconnected architecture on carbon cloth for high-performance flexible solid-state supercapacitors. Chem Eng J 391:12356
8. Wang J, Zhang X, Wei Q et al (2016) 3D self-supported nanopine forest-like Co_3O_4@$CoMoO_4$ core–shell architectures for high-energy solid state supercapacitors. Nano Energy 19:222–233
9. Guan Q, Cheng J, Wang B et al (2014) Needle-like Co_3O_4 Anchored on the graphene with enhanced electrochemical performance for aqueous supercapacitors. Acs Appl Mater Inter 6:7626–7632
10. Shi C, Wang X, Gao Y et al (2017) Nickel metal-organic framework nanoparticles as electrode materials for Li-ion batteries and supercapacitors. J Solid State Electrochem 21:2415–2423
11. Wu X, Meng L, Wang Q et al (2017) A flexible asymmetric fibered-supercapacitor based on unique Co_3O_4@PPy core-shell nanorod arrays electrode. Chem Eng J 327:193–201
12. Ma XJ, Kong LB, Zhang WB et al (2014) Design and synthesis of 3D Co_3O_4@$MMoO_4$ (M=Ni, Co) nanocomposites as high-performance supercapacitor electrodes. Electrochim Acta 130:660–669
13. Ouyang Y, Ye H, Xia X et al (2019) Hierarchical electrodes of $NiCo_2S_4$ nanosheets-anchored sulfur-doped Co_3O_4 nanoneedles with advanced performance for battery-supercapacitor hybrid devices. J Mater Chem A 7:3228–3237
14. Zhang C, Wei J, Chen L et al (2017) All-solid-state asymmetric supercapacitors based on Fe-doped mesoporous Co_3O_4 and three-dimensional reduced graphene oxide electrodes with high energy and power densities. Nanoscale 9:15423–15433
15. Li G, Chen M, Ouyang Y et al (2019) Manganese doped Co_3O_4 mesoporous nanoneedle array for long cycle-stable supercapacitors. Appl Surf Sci 469:941–950
16. Pu J, Shen Z, Zhong C et al (2019) Electrodeposition technologies for Li-based batteries: new frontiers of energy storage. Adv Mater 32:1903808
17. Chodankar NR, Dubal DP, Ji SH et al (2018) Superfast electrodeposition of newly developed $RuCo_2O_4$ nanobelts over low-cost stainless steel mesh for high-performance aqueous supercapacitor. Adv Mater Interfaces 5:1800283
18. Huang J, Wei J, Xiao Y et al (2018) When Al-doped cobalt sulfide nanosheets meet nickel nanotube arrays: a highly efficient and stable cathode for asymmetric supercapacitors. ACS Nano 12:3030–3041
19. Zhou X, Ren Y, Lu Y et al (2019) Porous Mo-Co-S nanosheets on carbon cloth for all-solid-state flexible asymmetric supercapacitors. Adv Mater Interfaces 6:1901138
20. Chen X, Liu B, Zhong C et al (2017) Ultrathin Co_3O_4 layers with large contact area on carbon fibers as high-performance electrode for flexible zinc-air battery integrated with flexible display. Adv Energy Mater 7:1700779
21. Yao D, Ouyang Y, Jiao X et al (2018) Hierarchical NiO@$NiCo_2O_4$ core-shell nanosheet arrays on Ni foam for high-performance electrochemical supercapacitors. Ind Eng Chem Res 57:6246–6256

22. Xuan W, Ramachandran R, Zhao C et al (2018) Influence of synthesis temperature on cobalt metal-organic framework (Co-MOF) formation and its electrochemical performance towards supercapacitor electrodes. J Solid State Electrochem 22:3873–3881
23. Li M, Wang Y, Yang H et al (2017) Hierarchical $CoMoO_4$@Co_3O_4 nanocomposites on an ordered macro-porous electrode plate as a multi-dimensional electrode in high-performance supercapacitors. J Mater Chem A 5:17312–17324
24. Zhang Z, Zhang H, Zhang X et al (2016) Facile synthesis of hierarchical $CoMoO_4$@$NiMoO_4$ core-shell nanosheet arrays on nickel foam as an advanced electrode for asymmetric supercapacitors. J Mater Chem A 4:18578–18584
25. Xia X, Hao Q, Lei W et al (2012) Reduced-graphene oxide/molybdenum oxide/polyaniline ternary composite for high energy density supercapacitors: synthesis and properties. J Mater Chem 22:8314–8320
26. Du W, Liu R, Jiang Y et al (2013) Facile synthesis of hollow Co_3O_4 boxes for high capacity supercapacitor. J Power Sources 227:101–105
27. Chen Y, Ei-Khouly ME, Sasaki M et al (2005) Synthesis of the axially substituted titanium Pc-C60 dyad with a convenient method. Org Lett 7:1613–1616
28. Hao Q, Xia X, Lei W et al (2015) Facile synthesis of sandwich-like polyaniline/boron-doped graphene nano hybrid for supercapacitors. Carbon 81:552–563
29. Yang C, Liu Q, Zang L et al (2019) High-performance yarn supercapacitor based on metal-inorganic-organic hybrid electrode for wearable electronics. Adv Electron Mater 5:1800435
30. Zhang C, Ke F, Xiao H et al (2019) Well-designed hollow and porous Co3O4 microspheres used as an anode for Li-ion battery. J Solid State Electrochem 23:2477–2482
31. Yang Z, Ma Q, Han L et al (2019) Design of Mo-doped cobalt sulfide hollow nanocages from zeolitic imidazolate frameworks as advanced electrodes for supercapacitors. Inorg Chem Front 6:2178–2184
32. Zhu Y, Du W, Zhang Q et al (2020) A metal-organic framework template derived hierarchical Mo-doped LDHs@MOF-Se core-shell array electrode for supercapacitors. Chem Commun 56:13848–13851
33. Zhao Y, He X, Chen R et al (2018) A flexible all-solid-state asymmetric supercapacitors based on hierarchical carbon cloth@$CoMoO_4$@NiCo layered double hydroxide core-shell heterostructures. Chem Eng J 352:29–38
34. Zhang SW, Yin BS, Liu XX et al (2019) A high energy density aqueous hybrid supercapacitor with widened potential window through multi approaches. Nano Energy 59:41–49